

Increasing N_{eff} with particles in thermal equilibrium with neutrinos

Céline Boehm,^{1,2,*} Matthew J. Dolan,^{1,†} and Christopher McCabe^{1,‡}

¹*Institute for Particle Physics Phenomenology, Durham University,
South Road, Durham, DH1 3LE, United Kingdom*

²*LAPTH, U. de Savoie, CNRS, BP 110, 74941 Annecy-Le-Vieux, France*

(Dated: November 27, 2024)

Recent work on increasing the effective number of neutrino species (N_{eff}) in the early universe has focussed on introducing extra relativistic species ('dark radiation'). We draw attention to another possibility: a new particle of mass $\lesssim 10$ MeV that remains in thermal equilibrium with neutrinos until it becomes non-relativistic increases the neutrino temperature relative to the photons. We demonstrate that this leads to a value of N_{eff} that is greater than three and that N_{eff} at CMB formation is larger than at BBN. We investigate the constraints on such particles from the primordial abundance of helium and deuterium created during BBN and from the CMB power spectrum measured by ACT and SPT and find that they are presently relatively unconstrained. We forecast the sensitivity of the Planck satellite to this scenario: in addition to dramatically improving constraints on the particle mass, in some regions of parameter space it can discriminate between the new particle being a real or complex scalar.

I. INTRODUCTION

Observations of the abundance of light nuclei produced during big-bang nucleosynthesis (BBN) and precision measurements of temperature anisotropies in the cosmic microwave background (CMB) provide unique windows into the particle content of the early universe. Both epochs are sensitive to the expansion rate of the early universe, which depends on the number of relativistic species in thermal equilibrium. The number of relativistic species is usually parameterised in terms of N_{eff} , the number of effective neutrino species with a late-time neutrino-to-photon temperature ratio $T_\nu/T_\gamma = (4/11)^{1/3}$. In the standard cosmological model with three neutrino species, this temperature ratio is slightly higher than $(4/11)^{1/3}$ due to partial reheating of the neutrinos when electrons and positrons annihilate, leading to $N_{\text{eff}} = 3.046$ [1, 2]. A measurement of N_{eff} greater than this would be a clear sign of new physics.

BBN imposes limits on N_{eff} at a photon temperature around 1 – 0.1 MeV, since increasing N_{eff} leads to a higher abundance of primordial helium and deuterium [3]. While the determination of these light nuclei from astrophysical observations is not yet completely settled, the latest data show a preference for a value of N_{eff} greater than three. For instance, ref. [4] finds $N_{\text{eff}} = 3.7^{+0.8}_{-0.7}$ (2σ) from their inferred abundance of primordial ^4He . An independent determination of N_{eff} can be made at photon decoupling (when the photon temperature is around 1 eV) from the Silk damping [5] tail of the CMB power spectrum. The Atacama Cosmology Telescope (ACT) [6] and the South Pole Telescope (SPT) [7] have measured this damping

tail and, in combination with data from the Wilkinson Microwave Anisotropy Probe (WMAP) [8], baryon acoustic oscillations (BAO) [9] and the Hubble constant (H_0) [10, 11], also find a preference for a value of N_{eff} greater than three, obtaining $N_{\text{eff}} = 4.6 \pm 0.8$ (1σ) and $N_{\text{eff}} = 3.9 \pm 0.4$ (1σ) respectively. Furthermore, various independent analyses of recent cosmological data find evidence for $N_{\text{eff}} > 3$ at 95% CL [12–16].

Given these hints for extra energy density in the early universe and bearing in mind the expectation that the Planck experiment will soon provide a significantly improved measurement of N_{eff} at photon decoupling (e.g. see [17]), we consider it a pertinent time to consider models in which N_{eff} is increased. The conventional way is to introduce extra 'dark' radiation, which leads to the same value of N_{eff} at BBN and photon decoupling (see e.g. [18–20]). While it is usually assumed that N_{eff} does not change between BBN and photon decoupling, intriguingly, the experimental data are consistent with a slightly larger value of N_{eff} at photon decoupling. This increase in N_{eff} after BBN can be achieved through decays to dark radiation during or after BBN (see e.g. [21–26]) or from primordial gravitational waves [27].

In this paper we explore another scenario that has received less attention in the literature, which predicts a value of N_{eff} greater than three, and moreover, predicts that N_{eff} at photon decoupling is larger than the value during BBN. As we will show in section II, N_{eff} scales as $(T_\nu/T_\gamma)^4$ so increasing the neutrino-to-photon temperature ratio leads to an increase in N_{eff} . A relative increase in T_ν/T_γ can be achieved by reducing the photon temperature relative to the neutrino temperature or by increasing the neutrino temperature relative to the photon temperature. A decrease in T_γ can be obtained through the production of hidden photons [28, 29] while a new light mediator may lead to a change in either T_γ or T_ν [30]. In this paper we follow the example of the standard cosmological model to increase T_ν : in the standard cosmological

*c.m.boehm@durham.ac.uk

†m.j.dolan@durham.ac.uk

‡christopher.mccabe@durham.ac.uk

model, the photons are hotter than the neutrinos because the transfer of entropy from the electrons and positrons to the photons (when they become non-relativistic) happens after the neutrinos decouple from the electromagnetic plasma at $T_D \approx 2.3$ MeV [31]. In an analogous way, we show that an additional ‘generic’ particle χ that remains in thermal equilibrium solely with the neutrinos after they decouple from the electromagnetic plasma and until it is non-relativistic, reheats the neutrinos relative to the electromagnetic plasma and as a result, leads to a higher value for N_{eff} . Requiring that the neutrino reheating, which happens when χ becomes non-relativistic and transfers its entropy to the neutrinos, happens after neutrino decoupling implies that χ must have a mass $m_\chi \lesssim \text{few} \cdot T_D \sim 10$ MeV.

The goal of this paper is to investigate the current and future constraints on χ from the inferred values of N_{eff} from BBN and the CMB. The only condition that we impose on the ‘generic’ particle χ is that the neutrino- χ interaction rate is sufficiently high that they remain in thermal equilibrium until χ is non-relativistic. Therefore, the constraints we derive may apply to, for instance, light dark matter particles that obtain their abundance from thermal freeze out (see e.g. [32–35]) or light mediators that have large couplings to neutrinos (see e.g. [36, 37]). The parameter that determines N_{eff} is m_χ as this dictates the additional energy density, so it is this parameter that we will constrain. During BBN, the photon temperature is similar to m_χ so χ makes a direct contribution to N_{eff} . In addition, there may also be an indirect contribution from the increase in T_ν/T_γ . At photon decoupling, we assume χ is non-relativistic so its direct contribution to N_{eff} is Boltzmann suppressed; the increase in N_{eff} arises solely from the increase in T_ν/T_γ . As we show in section II, this difference in the origin of the extra energy density leads to a larger value of N_{eff} at photon decoupling.

This paper is organised as follows. In section II we discuss the impact of light particles in thermal equilibrium with neutrinos on the energy density and neutrino-to-photon temperature ratio (some results are fully derived in an Appendix). Using these results, we first find the effect of χ on the abundance of primordial nuclei produced during BBN. This has previously been studied in [38, 39]. Here, we independently calculate the primordial abundance of ^4He and D/H as a function of m_χ and compare with recent experimental measurements. Our calculation uses a more recent BBN code than [38, 39] and includes the most recent values of the neutron lifetime and baryon density. We then calculate the value of N_{eff} as a function of m_χ at photon decoupling and compare with the experimental values inferred by ACT and SPT. Turning to consider experimental results from the near future, in section III we forecast the constraints that will soon be placed on χ from Planck’s measurement of N_{eff} . Finally, we conclude in section IV.

II. CURRENT CONSTRAINTS

The total energy density of the universe ρ_R is usually parameterised in terms of the energy density of photons ρ_γ , and the effective number of neutrinos N_{eff} with the usual neutrino-to-photon temperature ratio T_ν^0/T_γ (we define this ratio more carefully below)

$$\rho_R = \rho_\gamma \left[1 + \frac{7}{8} \left(\frac{T_\nu^0}{T_\gamma} \right)^4 N_{\text{eff}} \right]. \quad (1)$$

We are interested in the case where an additional particle χ with g_χ internal degrees of freedom and mass m_χ is in thermal equilibrium with the neutrinos. As the particles are in thermal equilibrium, they share a common temperature T_ν , which will in general be different from T_ν^0 . The resulting energy density of N_ν neutrinos and the additional particle χ is

$$\rho_{\nu:\chi} = \rho_\gamma \cdot \frac{7}{8} \left(\frac{T_\nu}{T_\gamma} \right)^4 \left[N_\nu + \frac{g_\chi}{2} I(y_\nu) \right], \quad (2)$$

where for convenience, we have defined $y_\nu \equiv m_\chi/T_\nu$ and the function

$$I(y) = \frac{120}{7\pi^4} \int_y^\infty d\xi \frac{\xi^2 \sqrt{\xi^2 - y^2}}{e^\xi \pm 1}, \quad (3)$$

which takes the limits $I(y \rightarrow \infty) = 0$ and $I(y \rightarrow 0) = 1$ (8/7) for fermions (bosons) (as usual, in eq. (3), -1 pertains to bosons and $+1$ to fermions). Comparing eq. (2) with the definition of N_{eff} in eq. (1), we see that

$$N_{\text{eff}}(y_\nu) = \left(\frac{T_\nu^0}{T_\gamma} \right)^{-4} \left(\frac{T_\nu}{T_\gamma} \right)^4 \left[N_\nu + \frac{g_\chi}{2} I(y_\nu) \right]. \quad (4)$$

In the Appendix, we use the conservation of entropy per-comoving-volume for particles in thermal equilibrium to show that (for $T_\gamma \leq T_D$)

$$\frac{T_\nu}{T_\gamma} = \left(\frac{g_{\star s:\nu} \Big|_{T_D}}{g_{\star s:\gamma} \Big|_{T_D}} \right)^{1/3}, \quad (5)$$

where $g_{\star s:\nu}$ and $g_{\star s:\gamma}$ are the effective number of relativistic degrees of freedom in the neutrino and electromagnetic sectors respectively and $\Big|_{T_D}$ indicates that $g_{\star s}$ should be evaluated at the neutrino decoupling temperature T_D . In the absence of χ , $g_{\star s:\nu}$ remains constant after decoupling, hence the usual neutrino-to-photon ratio is

$$\frac{T_\nu^0}{T_\gamma} = \left(\frac{g_{\star s:\gamma}}{g_{\star s:\nu} \Big|_{T_D}} \right)^{1/3}. \quad (6)$$

More generally, we see that

$$\left(\frac{T_\nu}{T_\gamma} \right) = \left(\frac{T_\nu^0}{T_\gamma} \right) \left(\frac{g_{\star s:\nu} \Big|_{T_D}}{g_{\star s:\nu}} \right)^{1/3}. \quad (7)$$

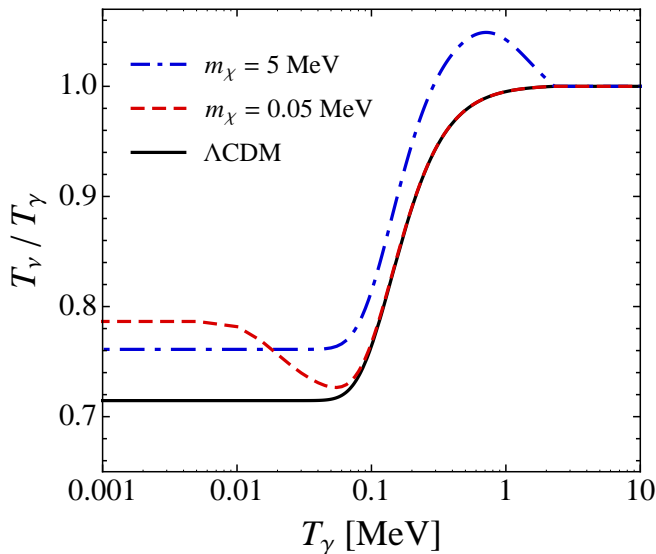


FIG. 1: The evolution of T_ν/T_γ with T_γ in the standard concordance model ‘ Λ CDM’ (black solid) and when there is an additional Majorana fermion in thermal equilibrium with neutrinos with mass $m_\chi = 5$ MeV (blue dot-dashed) and $m_\chi = 0.05$ MeV (red dashed). Neutrino reheating occurs when $T_\gamma \sim m_\chi$.

If χ becomes non-relativistic after decoupling, $g_{*s:\nu} < g_{*s:\nu}|_{T_D}$ and as a result, the neutrino-to-photon temperature ratio increases above its usual value. From eq. (4), we see that this leads to an increase in N_{eff} .

Finally, in the Appendix we show that eq. (7) can be written as

$$\left(\frac{T_\nu}{T_\gamma}\right) = \left(\frac{T_\nu^0}{T_\gamma^0}\right) \left[\frac{N_\nu + \frac{g_\chi}{2} F(y_\nu|_{T_D})}{N_\nu + \frac{g_\chi}{2} F(y_\nu)}\right]^{1/3}, \quad (8)$$

where $y_\nu|_{T_D} = m_\chi/T_D$ and we have defined the function

$$F(y) = \frac{30}{7\pi^4} \int_y^\infty d\xi \frac{(4\xi^2 - y^2)\sqrt{\xi^2 - y^2}}{e^\xi \pm 1}, \quad (9)$$

which takes the limits $F(y \rightarrow \infty) = 0$ and $F(y \rightarrow 0) = 1$ (8/7) for fermions (bosons). It is this form of T_ν/T_γ that we use in our calculations. In figure 1 we show how T_ν/T_γ evolves with T_γ for three cases: the black solid line shows the result from the standard concordance model with three neutrino species, in which the photon reheating occurs when $T_\gamma \sim m_e$; the blue dot-dashed and red dashed lines show the evolution when an additional Majorana fermion with mass $m_\chi = 5$ MeV and $m_\chi = 0.05$ MeV is in thermal equilibrium with the neutrinos. We see that the neutrino reheating occurs when $T_\gamma \sim m_\chi$. For the $m_\chi = 5$ MeV case, some of the reheating occurs for $T_\gamma \geq T_D$ during which the photons and neutrinos are reheated equally. In comparison, for

the $m_\chi = 0.05$ MeV case, all of the reheating occurs for $T_\gamma \leq T_D$ so only the neutrinos are reheated and therefore, the ratio of T_ν/T_γ is larger than the $m_\chi = 5$ MeV case at late times (small T_γ).

In the following subsections, we use the above formulae to explore the implications of χ on BBN and the CMB.

A. Effect on BBN

The abundance of ${}^4\text{He}$, expressed through the mass fraction Y_p , has long been recognised as a probe of the energy density present during BBN [40]. In the early universe the ratio of the neutron-to-proton number densities (n_n/n_p) is kept in thermal equilibrium through the weak interactions until the expansion rate becomes comparable to the weak interaction rate at $T \sim 0.7$ MeV. Increasing the expansion rate, by for instance introducing additional relativistic radiation, leads to a larger value of n_n/n_p at freeze out. Since essentially all of the neutrons present at $T \sim 0.1$ MeV are synthesised into ${}^4\text{He}$, introducing additional relativistic radiation therefore leads to a larger abundance of ${}^4\text{He}$. Similarly, increasing the expansion rate means that the reactions depleting the abundance of D freeze out earlier, leading to an increased abundance. The reactions that deplete D are more sensitive to the baryon-to-photon number density η and have historically been used to infer its value. However, if we use the value of η inferred by WMAP, then the number ratio D/H can be used along with Y_p as a measure of the energy density present during BBN, a point emphasised in [16]. Finally, the observed abundance of ${}^7\text{Li}$ remains $\sim 5\sigma$ away from the theoretical prediction, the so-called ‘lithium problem’ (for a recent review, see [41]). The modifications that we propose do not significantly alter the ${}^7\text{Li}$ abundance, therefore, in this work we directly compare our theoretical predictions with the inferred values Y_p and D/H from astrophysical measurements and make only passing reference to ${}^7\text{Li}$.

The impact on the primordial abundances of light nuclei from a generic particle χ that maintains thermal equilibrium with neutrinos throughout BBN has previously been considered in [38, 39]. Here we independently calculate Y_p and D/H using a modified version of the `ParthENoPE` BBN code [42]. We use the latest measurements of the baryon density $\Omega_b h^2 = 0.0223$, deduced from a joint analysis of SPT+WMAP7+ H_0 +BAO [7], and the PDG value of the neutron lifetime $\tau_n = 880.1$ s [43].

In the spirit of [39], we introduce a small temperature dependent parameter

$$\delta(T) \equiv 1 - \frac{T_\nu^0(T)}{T_\nu(T)}, \quad (10)$$

and perturb the `ParthENoPE` code in order to take into account the effects from the modified neutrino-to-photon temperature ratio. We use eq. (8) to calculate T_ν^0/T_ν . Typically, $\delta \sim 0.01$ and is always smaller than ~ 0.1 . A

non-zero value of δ increases the energy density of the neutrinos and enters into the phase-space of the weak interaction rates that determine n_n/n_p . The **ParthENoPE** interaction rates $\tilde{\Gamma}_{n \rightarrow p}$ and $\tilde{\Gamma}_{p \rightarrow n}$ include finite mass, QED radiative and finite temperature corrections. We calculate corrections to these rates in the Born approximation as an expansion in δ such that the total rate for $n \rightarrow p$ is given by

$$\Gamma_{n \rightarrow p}^{\text{total}} = \tilde{\Gamma}_{n \rightarrow p} + \epsilon_{n1}(T)\delta + \epsilon_{n2}(T)\delta^2 + \epsilon_{n3}(T)\delta^3, \quad (11)$$

where $\epsilon_{ni}(T)$ fits the change in the rates to an accuracy better than a few percent. A similar expression holds for the $p \rightarrow n$ rate. Finally, we also include the extra contribution to the energy density from χ , expressed in eq. (2).

The red dot-dashed, solid and dashed lines in figure 2 show our results for a complex scalar (B2), Majorana fermion (F2) and real scalar (B1) respectively as a function of m_χ . The upper and lower panels show the values of Y_p and D/H respectively and are in good qualitative agreement with those found in [38, 39], with slight differences due to the updated parameter values that we use. Although not shown here, our prediction for ${}^7\text{Li}$ is similar to that in [39]. For reference, the black dotted lines show the predicted values of Y_p and D/H for the indicated values of N_{eff} . As we would expect, for $m_\chi \gtrsim 15$ MeV, we recover the result from standard BBN: this is because χ is non-relativistic during BBN (so its contribution to the energy density is Boltzmann suppressed) and it has transferred its entropy to the neutrinos before they decouple from the photons, meaning that the standard neutrino-to-photon temperature ratio relation is maintained ($g_{*s:\nu} = g_{*s:\nu}|_{T_D}$ in eq. (7)). For $m_\chi \lesssim 0.05$ MeV, we asymptote to the result expected from a massless particle as χ remains relativistic throughout all of BBN. The values of Y_p and D/H for intermediate values of m_χ are a result of the direct contribution to the energy density from χ and the contribution from the modified neutrino-to-photon temperature ratio.

Recent inferences of Y_p from observations of metal-poor H II regions have been slightly higher than results from the past decade. For instance, while refs. [44] and [45] found $Y_p = 0.249 \pm 0.009$ and $Y_p = 0.2477 \pm 0.0029$ respectively, more recently, refs. [4], [46], [47] and [48] found $Y_p = 0.2565 \pm 0.0010(\text{stat.}) \pm 0.0050(\text{syst.})$, $Y_p = 0.2561 \pm 0.0108$, $Y_p = 0.2573^{+0.0033}_{-0.0088}$ and $Y_p = 0.2534 \pm 0.0083$ respectively, in good agreement with each other. The agreement of these recent results is perhaps not surprising as they originate from independent analyses of subsets of the data compiled in ref. [49]. However, all of these numbers serve to highlight that the value of Y_p is dominated by systematic errors. Therefore, following [50], we take the value of Y_p from ref. [4] with the statistical and systematic errors combined linearly: $Y_p = 0.2565 \pm 0.006$. The blue shaded region in the upper panel of figure 2 shows this 1σ region.

The experimental value for the number ratio D/H shows a large spread with the dispersion in the measure-

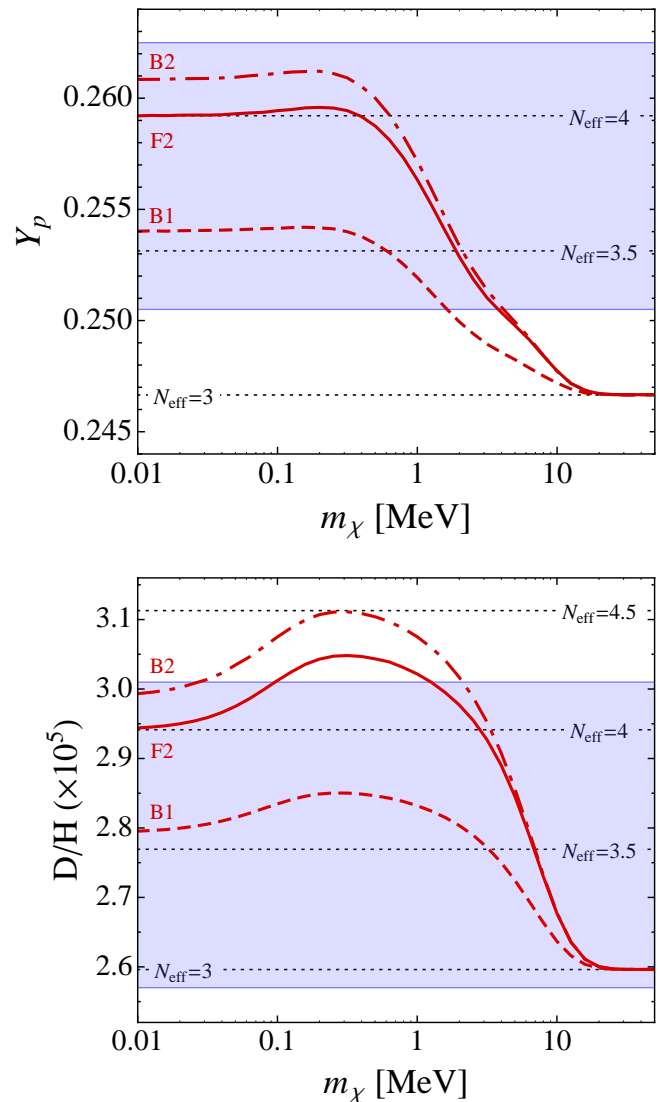


FIG. 2: The red dot-dashed, solid and dashed lines show the predictions for Y_p (upper panel) and D/H (lower panel) for a complex scalar (B2), Majorana fermion (F2) and real scalar (B1) respectively. The blue shaded region indicates the 1σ region for Y_p from [4] (with statistical and systematic errors combined linearly) and the 1σ weighted mean of D/H from [51]. The black dotted lines show the values of Y_p and D/H for the indicated values of N_{eff} .

ments well in excess of the quoted errors. For example, measurements range from $\text{D}/\text{H} \times 10^5 = 1.17^{+0.48}_{-0.34}$ in [52] to $\text{D}/\text{H} \times 10^5 = 3.98^{+0.70}_{-0.59}$ in [53]. Here we take as a conservative value $\text{D}/\text{H} \times 10^5 = 2.78^{+0.23}_{-0.21}$, the weighted mean calculated from eight independent samples in [51]. The blue shaded region in the lower panel of figure 2 shows this 1σ region. It is clear from figure 2 that the error on the measurements of Y_p and D/H are sufficiently large that all values of m_χ are currently consistent with the data at just over 1σ . Although the mea-

sured errors of Y_p are unlikely to improve considerably in the near future, recently, a precise measurement of D/H was presented with an error ~ 4 times smaller than the previous best [54]. With this measurement, they find that the weighted mean from ten independent samples is $D/H \times 10^5 = 2.63 \pm 0.12$ (where the shift in the weighted mean and reduction of the error is largely due to the new measurement in [54]). Comparing with the lower panel of figure 2, we see that this result disfavors $m_\chi \lesssim 4$ MeV at 2σ for a Majorana fermion and complex scalar while still allowing all values of m_χ for a real scalar. With further observations from metal-poor damped Lyman alpha systems of the type considered in [54], the large dispersion in the measurements of D/H would decrease and provide a strong, reliable constraint on this scenario.

B. Effect on the CMB

An independent determination of N_{eff} can be made from the CMB, which is at a much lower photon temperature than found during BBN. For the values of m_χ that we consider, χ 's direct contribution to the energy density is Boltzmann suppressed at photon decoupling ($T_{\gamma\text{-dec}} \sim 1$ eV): that is, $I(m_\chi/T_{\gamma\text{-dec}}) \simeq 0$ in eq. (2). However, assuming that χ remains in thermal equilibrium with neutrinos until it is non-relativistic, we can calculate its indirect contribution from the increase in the neutrino-to-photon temperature ratio from eq. (8) and the resulting value of N_{eff} from eq. (4). At photon decoupling we have $F(m_\chi/T_{\gamma\text{-dec}}) \simeq 0$ so N_{eff} is given by

$$N_{\text{eff}}|_{\text{CMB}} \simeq 3.046 \left[1 + \frac{g_\chi}{2} \frac{F(y_\nu|_{T_D})}{3.046} \right]^{4/3}, \quad (12)$$

where we have set $N_\nu = 3.046$ [1]. In figure 3 we show N_{eff} as a function of m_χ for a complex scalar (B2), Majorana fermion (F2) and real scalar (B1) in red dot-dashed, solid and dashed lines respectively. For $m_\chi \gtrsim 15$ MeV we recover the usual value for N_{eff} because the reheating effect from χ takes place before T_D , so the neutrinos and photons are both reheated equally. For $m_\chi \lesssim 2$ MeV, N_{eff} remains constant because the neutrinos are maximally reheated for all of these values of m_χ . This is because χ becomes non-relativistic after T_D and is fully non-relativistic by photon decoupling, therefore, all entropy from χ is transferred to the neutrinos. Naively, we might have expected N_{eff} to asymptote to four when χ is a light Majorana fermion. That this does not happen can be traced to the fact that the term in square brackets in eq. (12) is raised to a power $4/3$, rather than 1. This in turn follows from entropy conservation; the factor of 3 follows from the fact that $S \sim g_{*s} T^3$ is conserved, rather than $g_{*s} T^4$.

Experimentally, $N_{\text{eff}}|_{\text{CMB}}$ is determined from the CMB power spectrum at high multipole ℓ ('the Silk damping tail'). Increasing N_{eff} increases the energy density, which in turn increases the expansion rate.

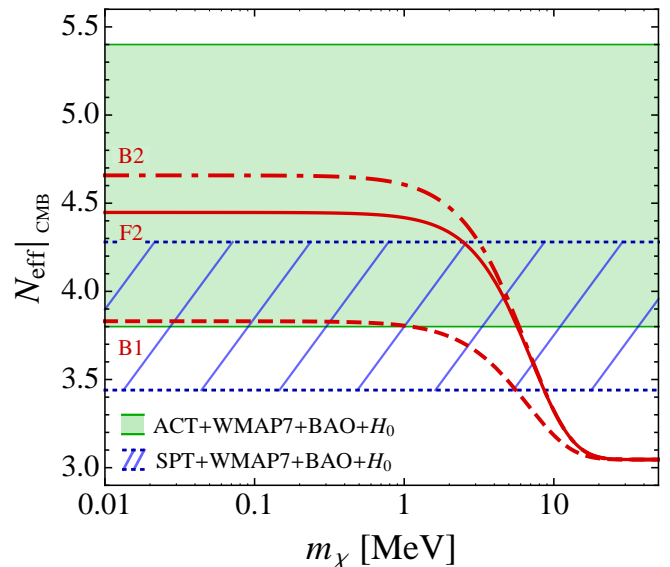


FIG. 3: The red dot-dashed, solid and dashed lines show N_{eff} at photon decoupling ($N_{\text{eff}}|_{\text{CMB}}$) as a function of m_χ for a complex scalar (B2), Majorana fermion (F2) and real scalar (B1) respectively. The shaded green and blue hatched regions show the 1σ range of N_{eff} determined from ACT and SPT (in combination with data from WMAP7, BAO and H_0) respectively.

As discussed in [55], an increased expansion rate leads to increased Silk damping which reduces the power in damping tail of the CMB power spectra. Currently, ACT [6] and SPT [7] provide the most precise measurements of the CMB power spectra at high ℓ (up to $\ell \sim 3000$) and are thus able to set the best limits on $N_{\text{eff}}|_{\text{CMB}}$ from the CMB power spectrum. In figure 3, we show the current 1σ constraints on $N_{\text{eff}}|_{\text{CMB}}$ from ACT (shaded green region) and SPT (blue hatched region) when their respective data sets are combined with data from WMAP7+BAO+ H_0 .¹ While we see that the ACT and SPT data show a preference for $N_{\text{eff}} > 3$ and therefore, $m_\chi \lesssim 10$ MeV, all values of m_χ are currently consistent with the data at 2σ . As a result, no strong conclusions on the preferred values of m_χ can currently be drawn from the data.

C. Comparison

Comparing figures 2 and 3, we see that $N_{\text{eff}}|_{\text{BBN}}$ and $N_{\text{eff}}|_{\text{CMB}}$ differ for the same value of m_χ . In figure 4 we

¹ Strictly speaking, these constraints apply when Y_p is fixed to the standard BBN value with N_{eff} massless fermions. However, from table I, we see that the constraints on $N_{\text{eff}}|_{\text{CMB}}$ (from SPT+WMAP7+BAO+ H_0) do not significantly change when Y_p is left as a free parameter.

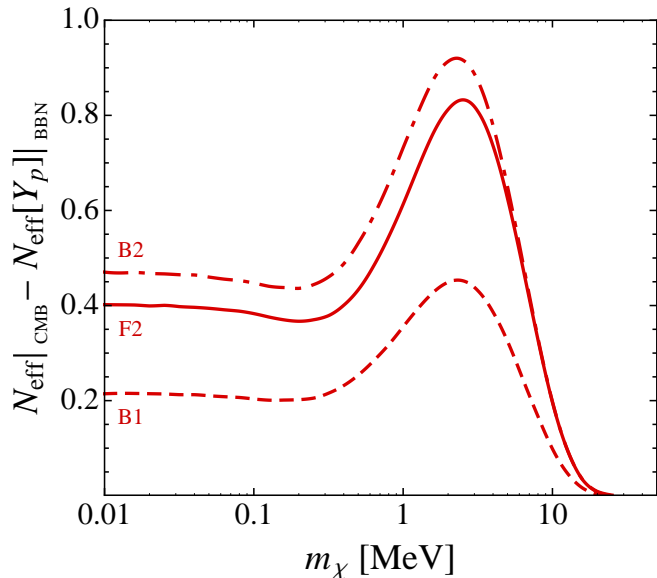


FIG. 4: The difference in N_{eff} at photon decoupling and BBN (inferred from the value of Y_p). The red dot-dashed, solid and dashed lines show the prediction for a complex scalar (B2), Majorana fermion (F2) and real scalar (B1) respectively.

explicitly show the difference in N_{eff} between the BBN and the CMB epochs as a function of m_χ for a complex scalar (B2), Majorana fermion (F2) and real scalar (B1) (in red dot-dashed, solid and dashed lines respectively). Here, we follow the usual convention and use the inferred value of $N_{\text{eff}}|_{\text{BBN}}$ from Y_p ($N_{\text{eff}}[Y_p]|_{\text{BBN}}$) but note that a similar figure could be drawn in which $N_{\text{eff}}|_{\text{BBN}}$ is inferred from the values of D/H. When a particle χ remains in thermal equilibrium with neutrinos until non-relativistic, we see that $N_{\text{eff}}|_{\text{CMB}} \geq N_{\text{eff}}[Y_p]|_{\text{BBN}}$. The equality holds for $m_\chi \gtrsim 15$ MeV because N_{eff} remains at its usual value. For $m_\chi \lesssim 0.2$ MeV, the difference is essentially constant because N_{eff} takes the maximum value at BBN and photon decoupling. The difference in N_{eff} is greatest for intermediate values of m_χ .

Finally, for completeness we mention a way to achieve $N_{\text{eff}}|_{\text{CMB}} \leq N_{\text{eff}}[Y_p]|_{\text{BBN}}$. If χ decouples from the neutrinos while still relativistic but after BBN (implying $m_\chi \lesssim 0.1$ MeV) we would have $N_{\text{eff}}[Y_p]|_{\text{BBN}} = 4$ and no reheating of the neutrinos would occur. Furthermore, if $m_\chi \gtrsim 1$ eV, χ would not contribute to the energy density at photon decoupling since it would be non-relativistic. Therefore, $N_{\text{eff}}|_{\text{CMB}} = 3.046$ as usual. We will not explore this possibility any further.

III. PLANCK FORECAST

In the previous section, we demonstrated in figures 2 and 3 that all values of m_χ are consistent (within 2σ) with the current measurements of N_{eff} from BBN and

the CMB for a particle χ , which remains in thermal equilibrium with the neutrinos after they decouple from the electromagnetic plasma and until it is non-relativistic. However, we would ideally like to place strong constraints on m_χ or find evidence for such a scenario. As Planck will soon provide significantly improved measurements of the CMB temperature anisotropy, we now turn to forecast its sensitivity to our scenario.

In section IIB we stated that N_{eff} is determined from measurements of the damping tail of the CMB power spectrum. Due to the accuracy of Planck, we must be careful to take into account other parameters that also lead to additional damping of power on small scales as they will be degenerate with N_{eff} [56]. For instance, a negative running of the spectral index n_s with scale k is one such parameter. However, the value required to provide sufficient damping, $dn_s/d\ln k \sim -0.02$, is much larger than expected from slow-roll inflationary models and would require a rethink of inflation and the generation of perturbations [57, 58] so we will not consider it further. Other examples of such parameters like an alternative model of dark energy, are considered in [59, 60]. Here, we concentrate on a conventional, flat, Λ CDM model that we extend to include a parameter that has already been central to our discussion, namely, Y_p . Since ${}^4\text{He}$ recombines earlier than hydrogen, increasing the ${}^4\text{He}$ abundance (at fixed baryon density) leads to fewer free electrons during hydrogen recombination. This in turn leads to a larger photon diffusion length and as a result, less power in the CMB damping tail [61]. Increasing N_{eff} can be compensated by decreasing Y_p so these parameters are degenerate [56].

In the first column of table I we list the cosmological parameters that we specify in our forecasts. In addition to $\Omega_b h^2$, n_s , N_{eff} and Y_p which have previously been defined, we choose values for the cold dark matter density $\Omega_{\text{DM}} h^2$; the reduced Hubble parameter h ; the angular scale of the sound horizon at last scattering θ_S ; ² the optical depth to reionization τ ; the amplitude of primordial scalar fluctuations $\ln[10^{10} A_S]$ (at a pivot scale $k = 0.002$ Mpc⁻¹) and the fraction of dark matter in the form of neutrinos $f_\nu = \Omega_\nu / \Omega_{\text{DM}}$. Finally, we also list the parameter σ_8 , the amplitude of linear matter fluctuations on scales of $8h^{-1}$ Mpc at $z = 0$, which is constrained by galaxy clusters.

In order to find the current best fit values for our parameters, we perform a fit with CosmoMC [62] to the SPT+WMAP7+BAO+ H_0 data. We use v4.1 of the WMAP likelihood code and v1.2 of the SPT likelihood code publicly available from the LAMBDA website [63]. Following [7], when calculating the SPT likelihood we also sample over three foreground nuisance parameters,

² In generating the mock data with CAMB, we choose h and θ_S is derived. In exploring the parameter space with CosmoMC, we sample over θ_S and h is derived. For completeness we list the values for both parameters.

Parameter	SPT+BAO+	Fiducial values		Prior range
	WMAP7+ H_0	Λ CDM	Λ CDM+ χ	
$100\Omega_b h^2$	2.27 ± 0.044	2.23	2.27	$0.5 \rightarrow 10$
$\Omega_{\text{DM}} h^2$	0.130 ± 0.0119	0.111	0.134	$0.01 \rightarrow 0.99$
h	0.73 ± 0.022	0.71	0.76	$0.4 \rightarrow 1.0$
$100\theta_S$	1.040 ± 0.0030	1.043	1.039	$0.5 \rightarrow 10$
τ	0.090 ± 0.015	0.09	0.09	$0.01 \rightarrow 0.8$
$\ln[10^{10} A_S]$	3.17 ± 0.04	3.17	3.16	$2.7 \rightarrow 4$
n_S	0.989 ± 0.013	0.98	0.99	$0.5 \rightarrow 1.5$
f_ν	< 0.054	0.008	0.020	$0 \rightarrow 1$
N_{eff}	3.98 ± 0.61	3.046	4.418	$2 \rightarrow 7$
Y_p	0.2629 ± 0.039	—	—	$0 \rightarrow 1$
	—	0.247	0.257	$0.22 \rightarrow 0.284$
σ_8	0.801 ± 0.054	0.803	0.816	—

TABLE I: The first column lists the cosmological parameters we sample over in our Planck forecast. The second column shows the values we obtain for these parameters when fitting to the SPT+WMAP7+BAO+ H_0 dataset. For two-tailed distributions the 68% CL is given while for one-tailed distributions, the upper 95% CL is given. In the third and fourth column we list the fiducial values of the various parameters chosen to generate the mock CMB data. ‘ Λ CDM’ corresponds to a cosmology without χ while in ‘ Λ CDM+ χ ’, Y_p and N_{eff} take the values for a 1 MeV Majorana fermion. The last column lists the flat priors we use in `CosmoMC`.

in addition to the cosmological parameters listed in table I. Here, Y_p is left free, with a top hat prior ranging from 0 to 1. The results of our fit are shown in the second column of table I. They are in good accord with similar results found in [59].

To generate mock CMB data, we follow [64, 65] and use the `FUTURCMB` [66] add-on package to `CosmoMC`. We use the `CAMB` software [67] package to obtain angular power spectra for the CMB anisotropies. From this we use the TT , TE and EE angular spectra for multiples $2 \leq \ell \leq 2500$, and the lensing deflection maps for dd and Td . Planck’s B -mode measurement will likely be noise-dominated so we omit it from our fits. We assume a sky coverage of $f_{\text{sky}} = 0.65$ and follow [65] in our approach to forecasting by replacing the power spectrum of the mock data by the fiducial data set. Using `CosmoMC`, we generate eight Markov chains in parallel and monitor the convergence with the Gelman-Rubin R -statistic [68], requiring that $R - 1 \leq 0.015$.

In the third and fourth columns of table I we list the fiducial values of the various parameters that we use to generate our mock CMB data. These are chosen to be consistent at or just outside the 1σ error range of the parameters in the second column. In the third column (‘ Λ CDM’), Y_p and N_{eff} are set to the values predicted from the standard concordance model. In the fourth column (‘ Λ CDM+ χ ’), Y_p and N_{eff} take the values expected from a 1 MeV Majorana fermion (as determined from

figures 2 and 3 respectively). In the fifth column we list the flat priors which we impose on the various parameters when exploring the parameter space with `CosmoMC`. In this case, we choose a conservative flat prior on Y_p . We assume that $Y_p < Y_\odot^{\text{ini}}$, where Y_\odot^{ini} is the initial solar abundance of helium, for which we take $Y_\odot^{\text{ini}} = 0.284$, the upper end of the 1σ range from [69]. Our lower bound $Y_p > 0.22$ is chosen as it is smaller than all values of Y_p determined from the large data set collated in [49]. Finally, we have chosen parameters to be within 2σ of the observed value of σ_8 : ref. [70] found $\sigma_8(\Omega_m/0.25)^{0.47} = 0.813 \pm 0.013(\text{stat.}) \pm 0.024(\text{syst.})$, where Ω_m is the matter density. We have that $\sigma_8(\Omega_m/0.25)^{0.47} = 0.827$ and 0.855 for ‘ Λ CDM’ and ‘ Λ CDM+ χ ’ respectively.

In figure 5 we show the results of our forecast in the Y_p - N_{eff} plane. The blue contours in the upper and lower panels of figure 5 show the 1σ and 2σ regions we find for Planck, after sampling over the mock power spectra created with the ‘ Λ CDM’ and ‘ Λ CDM+ χ ’ fiducial values from table I respectively.³ In both panels, the red dot-dashed, solid and dashed lines show the relation between Y_p and N_{eff} in the Y_p - N_{eff} plane for a particle χ when it is a complex scalar (B2), real scalar (B1) or Majorana fermion (F2) respectively. In the lower panel we have adjusted the scale of the vertical axis so as to better resolve these lines. Comparing with figures 2 and 3, it is clear that the left (right) edge of the lines correspond to the values of Y_p and N_{eff} for large (small) values of m_χ .

In the upper panel of figure 5, in green we show the 1σ and 2σ regions after fitting to SPT+WMAP7+BAO+ H_0 . Confirming the conclusions from section IIB, we see that SPT+WMAP7+BAO+ H_0 does not place strong constraints on m_χ , with all values lying within the 2σ region. In comparison, Planck’s confidence regions are much smaller and allow much more discrimination between values of m_χ . For instance, if Planck makes a measurement of N_{eff} close to three, as in the upper panel of figure 5, we see that it is able to exclude at 2σ values of m_χ below 4.8 MeV for a real scalar, 7.4 MeV for a Majorana fermion and 7.5 MeV for a complex scalar.

In the lower panel of figure 5, the green regions show the 1σ and 2σ regions from the inferred value of Y_p from Izotov et. al. [4] with statistical and systematic errors combined linearly. The black dotted line marked DR indicates the usual relation between Y_p and N_{eff} for dark radiation in which $N_{\text{eff}}|_{\text{BBN}} = N_{\text{eff}}|_{\text{CMB}}$. The deviation from this relation for a real scalar, complex scalar and Majorana fermion occurs because $N_{\text{eff}}|_{\text{CMB}} \geq N_{\text{eff}}[Y_p]|_{\text{BBN}}$. If Planck finds evidence for a larger value of N_{eff} , we see that it will be challenging to distinguish

³ We do not show the one-dimensional distributions for the individual parameters as we are primarily interested in how well Planck can discriminate between different values of m_χ . The one dimensional distributions we find have a similar variance to those found in, for instance [65].

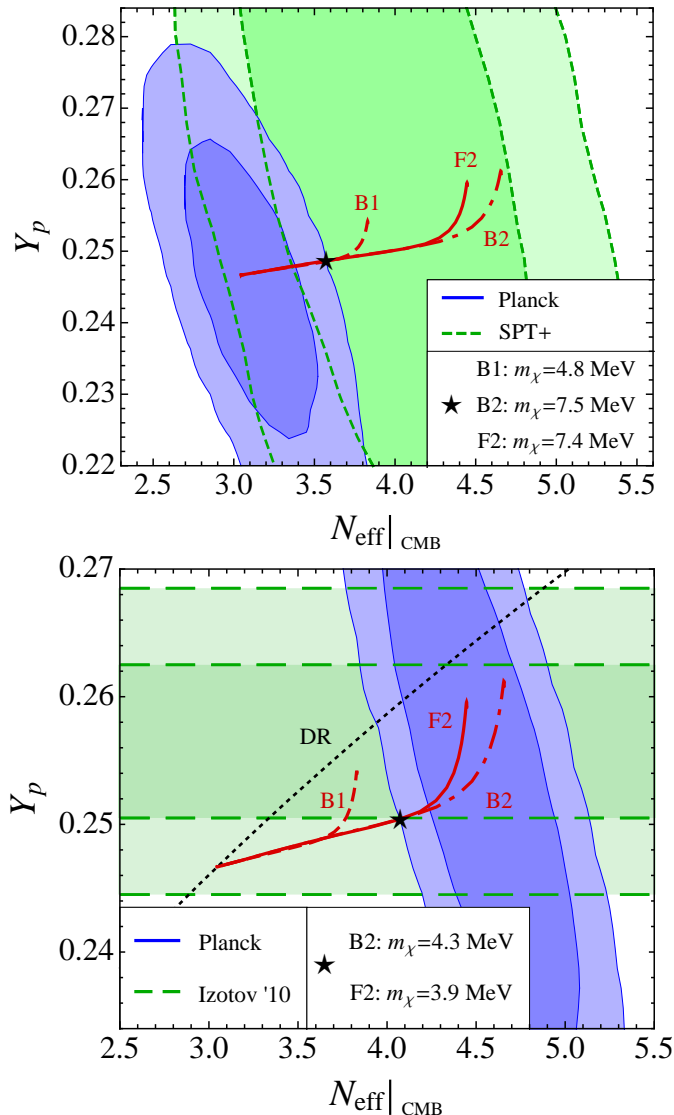


FIG. 5: The upper and lower panels correspond to the fiducial values of ‘ Λ CDM’ and ‘ Λ CDM+ χ ’ from table I respectively. Both panels: In blue are the Planck 1σ and 2σ regions. The red lines show the values of Y_p as a function of N_{eff} for a real scalar (B1), complex scalar (B2) and Majorana fermion (F2). The black star indicates the values of Y_p and N_{eff} for the stated values of m_χ in the box. Upper panel: In green are the SPT+WMAP7+BAO+ H_0 1σ and 2σ regions. Lower panel: In green are the 1σ and 2σ regions for Y_p from Izotov et. al. [4] (with statistical and systematic errors combined linearly). The black dotted line marked DR indicates the relation between Y_p and N_{eff} for dark radiation in which $N_{\text{eff}}|_{\text{BBN}} = N_{\text{eff}}|_{\text{CMB}}$.

between the case of dark radiation and a generic particle χ with high statistical significance unless the value of Y_p inferred from astrophysical measurements improves significantly. However, considering only particles in thermal equilibrium with neutrinos, we see that Planck is able to discriminate between a real scalar and a complex scalar

or Majorana fermion at more than 2σ and is able to exclude at 2σ values of m_χ heavier than 4.3 MeV for a complex scalar and 3.9 MeV for a Majorana fermion.

IV. CONCLUSIONS

Motivated by discrepancies in the determination of N_{eff} from BBN and the CMB, we have considered the impact of a new light particle which remains in thermal equilibrium with neutrinos until it becomes non-relativistic, which we assume occurs before photon decoupling. Such a particle leads to extra energy density in the early universe, either directly or through its effect on the ratio of the neutrino-to-photon temperature.

To quantify the impact of such particles on BBN, we updated the analysis of [38, 39] through modifications of the `ParthENoPE` code to take into account the two effects of light particles on the energy density mentioned above. These particles lead to an increased value of N_{eff} and bring the ${}^4\text{He}$ abundance into better agreement with recent observations (see the upper panel of figure 2). We also showed (in the lower panel of figure 2) that the D abundance is compatible with recent measurements.

We then considered the effect of such particles at the time of formation of the CMB. At this epoch, the increase in N_{eff} comes solely from the increase in the neutrino-to-photon temperature ratio, as χ is non-relativistic. As we showed in figure 3, this brings the value of N_{eff} into better agreement with the values reported by CMB experiments. In general, we found that the value of N_{eff} at the time of CMB formation is larger than the value at BBN. This is demonstrated explicitly in figure 4. Fixing Y_p to the value inferred from N_{eff} at photon decoupling, as is often done, is not applicable when setting constraints on this scenario.

As the current experimental constraints on our scenario are still relatively weak, we forecast the sensitivity of the Planck satellite to the effect of these particles on the CMB. We find that Planck is highly sensitive to the effects of such particles. If the value of N_{eff} derived from Planck agrees with that of standard cosmology with three neutrinos, we showed in the upper panel of figure 5 that it will rule out (for example) the existence of a light Majorana fermion with a mass of less than 7.4 MeV which couples to the neutrinos. The lower panel of figure 5 indicates that it will be difficult to distinguish between our scenario and the standard case of dark radiation (in which N_{eff} is the same at BBN and photon decoupling) at much more than 1σ when only data from astrophysical measurements of ${}^4\text{He}$ and Planck is considered. On the other hand, considering only particles in thermal equilibrium with neutrinos, we demonstrated in the lower panel of figure 5 that as well as providing significantly improved constraints on m_χ , in some regions of parameter space, Planck is even able to discriminate between a real scalar and a complex scalar or Majorana fermion.

Acknowledgments

We thank Daniel Albornoz Vásquez, Joanna Dunkley, Jeremy Mardon, Keith Olive and Subir Sarkar for discussions. MJD thanks the theory group at the University of Bonn for hospitality while some of this work was carried out.

Appendix A: Neutrino-to-photon temperature ratio

The energy density ρ and pressure p of a particle of mass m at temperature T and g internal degrees of freedom are given by (ignoring a possible chemical potential)

$$\rho = \frac{g T^4}{2\pi^2} \int_y^\infty d\xi \frac{\xi^2 \sqrt{\xi^2 - y^2}}{e^\xi \pm 1}, \quad (\text{A1})$$

$$p = \frac{g T^4}{6\pi^2} \int_y^\infty d\xi \frac{(\xi^2 - y^2)^{3/2}}{e^\xi \pm 1}, \quad (\text{A2})$$

where $\xi = E/T$, $y = m/T$ and here, as usual, -1 pertains to bosons and $+1$ to fermions.

In order to calculate the neutrino-to-photon temperature ratio, we use the conservation of entropy per comoving volume S for particles in thermal equilibrium with common temperature T . That is

$$S = a^3 \frac{\rho + p}{T} \equiv a^3 \frac{2\pi^2}{45} g_{*s} T^3 = \text{constant}. \quad (\text{A3})$$

Here, a is the scale factor and this equation defines g_{*s} , the effective number of relativistic degrees of freedom.

At $T = T_D$, the neutrinos and χ (the neutrino plasma) decouple from the electrons and photons (the electromagnetic plasma). From this point onwards, the neutrino and electromagnetic plasmas separately conserve comoving entropy. As a result, the neutrino and photon temperatures (T_ν and T_γ respectively) evolve according to

$$T_\nu = k_1 g_{*s:\nu}^{-1/3} a^{-1}, \quad (\text{A4})$$

$$T_\gamma = k_2 g_{*s:\gamma}^{-1/3} a^{-1}, \quad (\text{A5})$$

where k_1 and k_2 are constants and $g_{*s:\nu}$ and $g_{*s:\gamma}$ are the effective number of relativistic degrees of freedom in the neutrino and electromagnetic plasmas respectively. Assuming that the neutrinos and χ , and the photons and electrons decouple instantly at $T_\nu = T_\gamma = T_D$ (and ignoring that muon and tau neutrinos decouple slightly earlier than the electron neutrino [71]), we can determine k_1/k_2 and therefore, we find (for $T_\gamma < T_D$)

$$\frac{T_\nu}{T_\gamma} = \left(\frac{g_{*s:\nu} \Big|_{T_D}}{g_{*s:\gamma} \Big|_{T_D}} \right)^{1/3}, \quad (\text{A6})$$

where $|_{T_D}$ indicates that g_{*s} should be evaluated at T_D .

Using eqs. (A1) and (A2), the entropy per comoving volume for N_ν neutrinos and χ is

$$S_{\nu:\chi} = a^3 \frac{2\pi^2}{45} T_\nu^3 \cdot 2 \cdot \frac{7}{8} \cdot \left[N_\nu + \frac{g_\chi}{2} F(y_\nu) \right], \quad (\text{A7})$$

where $y_\nu \equiv m_\chi/T_\nu$ and for convenience, we have defined the function

$$F(y) = \frac{30}{7\pi^4} \int_y^\infty d\xi \frac{(4\xi^2 - y^2) \sqrt{\xi^2 - y^2}}{e^\xi \pm 1} \quad (\text{A8})$$

with limits, $F(y \rightarrow \infty) = 0$ and $F(y \rightarrow 0) = 1$ ($8/7$) for fermions (bosons). Comparing eq. (A7) with eq. (A3), it is straightforward to read off that

$$g_{*s:\nu} = 2 \cdot \frac{7}{8} \cdot \left[N_\nu + \frac{g_\chi}{2} F(y_\nu) \right]. \quad (\text{A9})$$

A similar argument shows that

$$g_{*s:\gamma} = 2 + 4 \cdot \frac{7}{8} \cdot F(z_e), \quad (\text{A10})$$

where $z_e \equiv m_e/T_\gamma$.

-
- [1] G. Mangano, G. Miele, S. Pastor, and M. Peloso, *Phys.Lett.* **B534** (2002), 8–16, [astro-ph/0111408].
- [2] G. Mangano, G. Miele, S. Pastor, T. Pinto, O. Pisanti, et al., *Nucl.Phys.* **B729** (2005), 221–234, [hep-ph/0506164].
- [3] S. Sarkar, *Rept.Prog.Phys.* **59** (1996), 1493–1610, [hep-ph/9602260].
- [4] Y. Izotov and T. Thuan, *Astrophys.J.* **710** (2010), L67–L71, [1001.4440].
- [5] J. Silk, *Astrophys.J.* **151** (1968), 459–471.
- [6] J. Dunkley, R. Hlozek, J. Sievers, V. Acquaviva, P. Ade, et al., *Astrophys.J.* **739** (2011), 52, [1009.0866].
- [7] R. Keisler, C. Reichardt, K. Aird, B. Benson, L. Bleem, et al., *Astrophys.J.* **743** (2011), 28, [1105.3182].
- [8] WMAP Collaboration, E. Komatsu et al., *Astrophys.J.Suppl.* **192** (2011), 18, [1001.4538].
- [9] SDSS Collaboration, W. J. Percival et al., *MNRAS* **401** (2010), 2148–2168, [0907.1660].
- [10] A. G. Riess, L. Macri, S. Casertano, M. Sosey, H. Lampeitl, et al., *Astrophys.J.* **699** (2009), 539–563, [0905.0695].
- [11] A. G. Riess, L. Macri, S. Casertano, H. Lampeitl, H. C. Ferguson, et al., *Astrophys.J.* **730** (2011), 119, [1103.2976].
- [12] T. L. Smith, S. Das, and O. Zahn, *Phys.Rev.* **D85** (2012), 023001, [1105.3246].

- [13] J. Hamann, S. Hannestad, G. G. Raffelt, and Y. Y. Wong, *JCAP* **1109** (2011), 034, [1108.4136].
- [14] M. Archidiacono, E. Calabrese, and A. Melchiorri, *Phys.Rev.* **D84** (2011), 123008, [1109.2767].
- [15] J. Hamann, *JCAP* **1203** (2012), 021, [1110.4271].
- [16] K. M. Nollett and G. P. Holder, (2011), 1112.2683.
- [17] S. Galli, M. Martinelli, A. Melchiorri, L. Pagano, B. D. Sherwin, et al., *Phys.Rev.* **D82** (2010), 123504, [1005.3808].
- [18] K. Nakayama, F. Takahashi, and T. T. Yanagida, *Phys.Lett.* **B697** (2011), 275–279, [1010.5693].
- [19] J. L. Feng, V. Rentala, and Z. Surujon, *Phys.Rev.* **D84** (2011), 095033, [1108.4689].
- [20] H. K. Dreiner, M. Hanussek, J. S. Kim, and S. Sarkar, *Phys.Rev.* **D85** (2012), 065027, [1111.5715].
- [21] K. Ichikawa, M. Kawasaki, K. Nakayama, M. Senami, and F. Takahashi, *JCAP* **0705** (2007), 008, [hep-ph/0703034].
- [22] W. Fischler and J. Meyers, *Phys.Rev.* **D83** (2011), 063520, [1011.3501].
- [23] J. Hasenkamp, *Phys.Lett.* **B707** (2012), 121–128, [1107.4319].
- [24] J. L. Menestrina and R. J. Scherrer, *Phys.Rev.* **D85** (2012), 047301, [1111.0605].
- [25] D. Hooper, F. S. Queiroz, and N. Y. Gnedin, *Phys.Rev.* **D85** (2012), 063513, [1111.6599].
- [26] O. E. Bjaelde, S. Das, and A. Moss, (2012), 1205.0553.
- [27] T. L. Smith, E. Pierpaoli, and M. Kamionkowski, *Phys.Rev.Lett.* **97** (2006), 021301, [astro-ph/0603144].
- [28] J. Jaeckel, J. Redondo, and A. Ringwald, *Phys.Rev.Lett.* **101** (2008), 131801, [0804.4157].
- [29] R. Foot, *Phys.Lett.* **B711** (2012), 238–243, [1111.6366].
- [30] M. Blennow, E. Fernandez-Martinez, O. Mena, J. Redondo, and P. Serra, *JCAP* **1207** (2012), 022, [1203.5803].
- [31] K. Enqvist, K. Kainulainen, and V. Semikoz, *Nucl.Phys.* **B374** (1992), 392–404.
- [32] C. Boehm, P. Fayet, and R. Schaeffer, *Phys.Lett.* **B518** (2001), 8–14, [astro-ph/0012504].
- [33] C. Boehm, T. Ensslin, and J. Silk, *J.Phys.G* **G30** (2004), 279–286, [astro-ph/0208458].
- [34] C. Boehm, Y. Farzan, T. Hambye, S. Palomares-Ruiz, and S. Pascoli, *Phys.Rev.* **D77** (2008), 043516, [hep-ph/0612228].
- [35] Y. Farzan, *Phys.Rev.* **D80** (2009), 073009, [0908.3729].
- [36] J. F. Beacom, N. F. Bell, and S. Dodelson, *Phys.Rev.Lett.* **93** (2004), 121302, [astro-ph/0404585].
- [37] S. Hannestad, *JCAP* **0502** (2005), 011, [astro-ph/0411475].
- [38] E. W. Kolb, M. S. Turner, and T. P. Walker, *Phys.Rev.* **D34** (1986), 2197.
- [39] P. D. Serpico and G. G. Raffelt, *Phys.Rev.* **D70** (2004), 043526, [astro-ph/0403417].
- [40] R. V. Wagoner, W. A. Fowler, and F. Hoyle, *Astrophys.J.* **148** (1967), 3–49.
- [41] B. D. Fields, *Ann.Rev.Nucl.Part.Sci.* **61** (2011), 47–68, [1203.3551].
- [42] O. Pisanti, A. Cirillo, S. Esposito, F. Iocco, G. Mangano, et al., *Comput.Phys.Commun.* **178** (2008), 956–971, [0705.0290].
- [43] Particle Data Group, J. Beringer et al., *Phys.Rev* **D86** (2012), 010001.
- [44] K. A. Olive and E. D. Skillman, *Astrophys.J.* **617** (2004), 29, [astro-ph/0405588].
- [45] M. Peimbert, V. Luridiana, and A. Peimbert, *Astrophys.J.* **666** (2007), 636–646, [astro-ph/0701580].
- [46] E. Aver, K. A. Olive, and E. D. Skillman, *JCAP* **1005** (2010), 003, [1001.5218].
- [47] E. Aver, K. A. Olive, and E. D. Skillman, *JCAP* **1103** (2011), 043, [1012.2385].
- [48] E. Aver, K. A. Olive, and E. D. Skillman, *JCAP* **1204** (2012), 004, [1112.3713].
- [49] Y. I. Izotov, T. Thuan, and G. Stasinska, *Astrophys.J.* **662** (2007), 15–38, [astro-ph/0702072].
- [50] G. Steigman, (2012), 1208.0032.
- [51] M. Fumagalli, J. M. O’Meara, and J. X. Prochaska, *Science* **334** (2011), 1245, [1111.2334].
- [52] R. Srianand, N. Gupta, P. Petitjean, P. Noterdaeme, and C. Ledoux, *MNRAS* **405** (2010), 1888–1900, [1002.4620].
- [53] S. Burles and D. Tytler, *Astrophys.J.* **507** (1998), 732–744, [astro-ph/9712109].
- [54] M. Pettini and R. Cooke, *MNRAS* **425** (2012), 2477, [1205.3785].
- [55] Z. Hou, R. Keisler, L. Knox, M. Millea, and C. Reichardt, (2011), 1104.2333.
- [56] S. Bashinsky and U. Seljak, *Phys.Rev.* **D69** (2004), 083002, [astro-ph/0310198].
- [57] A. Kosowsky and M. S. Turner, *Phys.Rev.* **D52** (1995), 1739–1743, [astro-ph/9504071].
- [58] D. Baumann, (2009), 0907.5424.
- [59] S. Joudaki, (2012), 1202.0005.
- [60] M. Archidiacono, E. Giusarma, A. Melchiorri, and O. Mena, *Phys.Rev.* **D86** (2012), 043509, [1206.0109].
- [61] G. Steigman, *JCAP* **1004** (2010), 029, [1002.3604].
- [62] A. Lewis and S. Bridle, *Phys. Rev.* **D66** (2002), 103511, [astro-ph/0205436].
- [63] <http://lambda.gsfc.nasa.gov>.
- [64] L. Perotto, J. Lesgourgues, S. Hannestad, H. Tu, and Y. Y. Wong, *JCAP* **0610** (2006), 013, [astro-ph/0606227].
- [65] J. Hamann, J. Lesgourgues, and G. Mangano, *JCAP* **0803** (2008), 004, [0712.2826].
- [66] Available from <http://lpsc.in2p3.fr/perotto>.
- [67] A. Lewis, A. Challinor, and A. Lasenby, *Astrophys.J.* **538** (2000), 473–476, [astro-ph/9911177].
- [68] A. Gelman and D. B. Rubin, *Statist.Sci.* **7** (1992), 457–472.
- [69] A. Serenelli and S. Basu, *Astrophys.J.* **719** (2010), 865–872, [1006.0244].
- [70] A. Vikhlinin, A. Kravtsov, R. Burenin, H. Ebeling, W. Forman, et al., *Astrophys.J.* **692** (2009), 1060–1074, [0812.2720].
- [71] F. Iocco, G. Mangano, G. Miele, O. Pisanti, and P. D. Serpico, *Phys.Rept.* **472** (2009), 1–76, [0809.0631].